Analytical Qualification of Composite Structures

G.A.O. Davies, D. Hitchings
Department of Aeronautics, Imperial College
South Kensington
London SW7 2BY
United Kingdom

Abstract

The feasibility of replacing substructure and component testing by analytical "virtual testing" is addressed here for composite structures. The special difficulties in estimating the failure loads of composite structures are described, especially when initiation starts from a local stress concentration. Damage may initiate and then propagate, but final failure can occur at a load significantly higher than that for initiation. The separate modes of in-plane (fibre-dominated) and delamination (matrix dominated) are shown to need different strength and fracture strategies. Several examples are chosen of realistic structures, ranging from notches through to stiffened compression panels, starting with the easiest (in-plane dominated) and finishing with the most difficult mixed in-plane and debonding case.

1. INTRODUCTION

The need to replace expensive structural testing by theoretical simulation is no longer a contentious issue. It is accepted. In fact it was first explored in 1990 by an AGARD workshop "Analytical Qualification of Aircraft Structures" [Ref 1]. Amongst its conclusions twelve years ago was that "composite structures are more sensitive to secondary effects than metallic structures and, as a result, require more detailed local analysis than is used for metallic structures to model critical failure mechanisms and predict failure reliably". However no one doubts that full-scale static and fatigue tests will always be obligatory for both civil and military aircraft. The use of real or virtual testing for substructures and components is a choice that can be left to the designers and manufacturers who need to save resources and time-to-market, but also need to ensure that the full scale test will confirm the design safety factors. Why then are we certain that full scale tests will always be obligatory, when modern finite element software can quite quickly create models starting from the digital pre-assembly? (or electronic mock-up) One reason is the uncertainty in predicting the fatigue life of safety-critical metallic primary structures. A FE model may miss out highly local stress concentrations which initiate cracks and which can then become unstable. This is one reason why full scale tests are not insisted by the airworthiness authorities for later versions of aircraft which may be "stretched" significantly from the original prototype. At least the stress concentrations will be the same even if the loading may be different.

Composite structures are even less likely to escape full scale tests for a reason similar to the above. Laminated high performance composite structures are ultra sensitive to local stress concentrations which give rise to 3-D stress fields having components in the "through-thickness" direction: the Achilles heel of composites structures. The sensitivity to local stress concentrations has led to excessive caution in defining the reliable stresses and strains. For example the design allowable compressive strain is often taken as 0.3% to 0.4% whereas a coupon test should survive at least twice these figures. Ironically the superior fatigue performance of composite structures may be due more to these conservative safety factors than to the durability of the basic material.

Paper presented at the RTO AVT Symposium on "Reduction of Military Vehicle Acquisition Time and Cost through Advanced Modelling and Virtual Simulation", held in Paris, France, 22-25 April 2002, and published in RTO-MP-089.

How then has industry managed to design reasonably safe and light composite structures? Basically the usual FE analysis is reliable enough to deliver local stresses/forces/moments in a global solution. However if there is any doubt about stress concentrations somewhere, a very local experimental test will be designed, such as a stiffener pull-off in a compression panel as illustrated in Figure 1. The loads causing failure will then be compared to the theoretical internal loads in the global FE solution.There are countless examples of detail and component tests being used as part of the design process for a new aircraft. It is the purpose of this paper to examine the capability of theoretical and software tools in evaluating the allowable loads in a local model, and so avoid the expensive testing of many such generic features.

One issue to be considered is whether the local allowable loads are valid anyway. The initiation of failure may lower the local stiffness so that the interface loads are themselves lowered. Thus can we ignore the coupling between the local and global structures? We will show that the use of local loads, not changing, is closer to the truth than using interface displacements, i.e. the surrounding structure has a very large reservoir of strain energy. Of course the initiation of failure in brittle composite structures may be unstable anyway and no local redistribution will save it. We will show that damage propagation away from the local stress concentration may be either unstable and rapid, or stable and then arresting, depending on the nature of the surrounding structure.

It should be mentioned that this local/global approach for composite structures is already being marketed by at least three commercial code developers.

- Alpha Star Corporation (GENOA) use strategies developed at NASA Ames.
- MERL use strategies developed at NASA Langley.
- ESI (PAM series)

Anecdotal evidence from industry is that these codes have limitations, and require considerable skill to use, that is the failure simulation is far from being an automatic routine. We will look at the problems of simulating failure and suggest the way forward.

2. FAILURE MECHANISMS

Restricting ourselves to laminated structures we have to differentiate between in-plane fibre-dominated failure and out-of-plane matrix-dominated (delamination or debonding). In-plane failures due to stress concentrations are not strictly amenable to fracture mechanics since in tension no sharp cracks develop: there is much blunting of a potential crack front with matrix cracking delamination and fibre bridging. In fact, unlike metals, a sharper crack front can develop under compression and the use of energy release rate criteria has been successful in estimating the compressive failure load in plates with circular holes [Ref 2]. In the absence of sharp cracks it is feasible to use a strength criteria, based on laminate stresses or strains. It is not the purpose of this paper to discuss the many empirical failure criteria, usually a polynomial in the various stress components for a uni-directional laminar. We assume that some criteria can be applied to a single ply in a laminated stack, and as the load is increased some first ply failure occurs at which the local stiffness in (say) a finite element, is put to zero or reduced to a negligible value. The load is then increased further and the pattern repeated so the damage propagates through the thickness and away from the source until eventual failure. The damage propagation is analogous to plasticity and limit loads in metallic structures. This approach has been successfully demonstrated for simple coupon tests [Ref 3] and we here show how it works for realistic structures.

The other failure mode is delamination and this is much more difficult to simulate in realistic structures. It does mean coping with a sharp crack and singularity, so strength criteria will not work. Fracture mechanics in some form has to be used, and the most direct way is to evaluate the strain energy release rate (SERR) by opening a crack or closing it, and comparing

with a known critical value determined by test. The main problem here is that the delamination crack front has to be moved and monitored. This is computationally expensive and the FE mesh size may have to be fine to evaluate the SERR accurately and capture the shape of the crack front as the applied load is increased. An alternative strategy is the use of interface elements, which may be dimensionless with zero thickness but whose force/displacement law captures the physics of crack propagation. We have used the model shown in Figure 2 for a crack of unit length. The slope of the rise could be a measure of say resin stiffness, and the strength a measure of allowable stress in tension (mode 1) or shear (mode 2). We have used a linear decay over the so called "process zone" but the important feature is that the area enclosed is equal to the critical SERR G_{IC} or G_{IIC}. The big advantage of interface elements is that no "flaw" is needed to start propagation, and no crack front is needed to monitor. The user of course has to insert complete areas of interface elements where delamination or debonding is thought likely.

Whether the failure is in-plane or delamination we recognise that the material is softening with a global stiffness change that may be negative-definite. This always causes numerical problems. It can even happen elastically in the case of compression panels taken beyond initial buckling when a mode change occurs. The structure may snap-through or even snap-back. We have therefore adopted the technique of simulating all failure events as dynamic, and using explicit integration. For static problems, even non-linear, it can be expensive to load incrementally and solve the dynamic response at each increment. It is therefore necessary to use fictitious mass and damping so that the static solution is reached as quickly as possible, thus a critically damping behaviour is aimed for. Consider the equations of motion for the displacement vector **r.**

$$\mathbf{M}\mathbf{r}'' + \mathbf{C}\mathbf{r}' + \mathbf{K}\mathbf{r} = \mathbf{0}$$

We choose proportional damping $\mathbf{C} = \alpha\mathbf{M} + \beta\mathbf{K}$, but it is impossible to choose the two parameters α and β to achieve critical damping over the full range of eigenfrequencies for large M and K. One strategy which works well is to put $\mathbf{M} = \mathbf{K}$. All undamped eigenvalues are then unity and critical damping can be achieved. However an even simpler strategy is to put $\mathbf{M} = \mathbf{0}$ and $\mathbf{C} = \mathbf{K}$. The single eigenvalue is now real and negative and we and if we have not achieved convergence in (say) 20 iterations, the step size is doubled.

Some examples of failure simulation are now illustrated, starting with the easiest pure in-plane fibre-dominated failures and proceeding through to the most difficult debonding in compression panels.

3. STRESS CONCENTRATIONS DUE TO CIRCULAR HOLES

This example is taken from a research program undertaken by a UK Industry/MoD Consortium, and aimed at evaluating the best criteria for predicting failure in carbon fibre panels with various sizes of circular holes and subjected to a biaxial stress field. It was known that strength would decrease with hole size, but, unlike brittle metals, linear elastic fracture mechanics will not work. We show here results for a biaxial field of equal tension (in the "x" direction) and compression (in the "y" direction). Attempts to explain failure using the local stress field and various "failure" stress criteria were not very successful as Figure 3 indicates, the experimental values being roughly twice those of the popular "point stress" criteria. The notched plates were surrounded by a reinforced structure leading to the load input points, details of which are actually confidential. However the net result was that damage initiation at the hole edge did not propagate in an unstable fashion, but the surrounding reinforcements

acted as effective crack inhibitors until final failure occurred at a later loading stage. The explicit degradation algorithm shows in Figure 4 the first loss of stiffness occurring at a load of 100kN, and eventually leading to total failure at a load of 138kN. (The small residual stiffness above this loading is due to assuming any ply stiffness retains 10% of its elastic value after failure, and is a device simply to avoid expensive convergent times.) The plots of damage in Figure 5 show an initial propagation along the x axis due to the lower compressive strength of the material but eventually the damage extends over the whole plate. (The patchy displays are due to the plotting routine!). Figure 6 summarises the effect of hole size and the agreement between test and prediction is satisfying. Delamination was not modelled in this exercise, although it does occur at the hole boundary, but it did not lead to buckling and propagation. The next example is also uninfluenced by delamination.

4. COMPRESSION AFTER IMPACT (CAI) STRENGTH OF SANDWICH PANELS

This example is a sandwich panel having carbon fibre skins and an aluminium alloy honeycomb core. This ductile core is a very good energy absorber of low velocity impact. The CAI behaviour depends on whether the skin is stiff enough, and the core interface weak, so that the skin recovers as shown in Figure 7 leaving an invisible void which makes the panel vulnerable. Compression loading can cause the unsupported skin to buckle which will then propagate in a mode 1 fashion. However if a strong core can hold the indentation, then applied compression will cause the indentation to push further into the core and increase the local bending strains. A point will eventually be reached when these strains reach the allowable strength values and the indentation will propagate rapidly as a narrow band right across the panel. Delamination plays no role in this history, and, to simulate the rapid propagation across the entire panel, we found it necessary to combine the local and global behaviour from the very start, simply using a refined mesh in the region of the impactor. Traditional Mindlin plate elements were used for the skins but individual plies were degraded by 90% when the Chang-Chang failure criteria was exceeded. The core was idealised as a homogenous elastoplastic medium with properties in compression, tension and shear found from experimental tests. The explicit routine was used to simulate the impact event and create damage and residual deformations, and then the same routine was used for the CAI strength simulation.

Figure 8 shows the force histories for an impact of 120J energy, confirming the validity of the model. The residual indentation was also predicted well. The model was then subjected to incremental compressive loading and at a value of 480kN the damage and deformation propagated suddenly in a narrow band right across the panel as shown in Figure 9. The predicted fibre damage map in Figure 10 shows this band on the damaged side which then lead to the panel pivoting across this "hinge" and starting to cause failure in the other skin. This damage band can be compared with the experimental C-scan in Figure 11 which shows the signal from the crushed core. The failure of 480kN compares with the test value of 505kN; and a value of 770kN for the undamaged panel.

5. COMPRESSION AFTER IMPACT STRENGTH OF CURVED PANELS

We now proceed to a problem where delamination cannot be ignored. If flat plates are subjected to low velocity impact it can be shown that the internal delamination is driven primarily by the magnitude of the impact force [Ref 4] which is greater the stiffer the plate. On the other hand fibre damage is driven mostly by the bending strains which will be large if the plate is very flexible. It has been common to assume that delamination does not affect the flexural stiffness much so that the impact force can be predicted allowing only for loss of stiffness due to fibre failure. Figure 12 shows how necessary it is to include this flexural stiffness degradation. However if a curved shell is impacted it will have a significantly higher stiffness and therefore impact forces, so it was necessary to see if delamination should be

included in the impact simulation, and also whether both flexural degradation and delamination should be included in the CAI simulation. The rigs chosen (Figure 13) were modifications to the standard Boeing impact and CAI test rigs. It was found that, for a thin 2mm curved panel, an impact of only 1.86J energy produced 900mm^2 delamination. (900mm^2 is a circle of diameter 340mm or 17 times the plate thickness). This compares with an area of only 300mm^2 for a flat plate subjected to a much larger 7J energy impact. The importance of recognising the loss of stiffness due to delamination was quickly established. In Figure 14 the force histories for 1.86J impact on the curved panels, are shown for the test results and the FE predictions. By modelling both fibre damage and delamination the maximum force of 1200N and the half-period of 3ms was captured well. However by ignoring delamination the stiffer structure has a half-period of only 2ms and the maximum force rises to 1800N.

Having created the internal damage by the FE code FE77, it is then possible to load in compression the damaged structure once more. It should be mentioned that it is important to start applying loading to the damaged but static structure, and it was found necessary to increase the artificial damping once the impact mass had left the structure, to avoid a long computational time for the free vibrations to disappear. Figure 15 shows the FE model and the history of displacements as the compressive load is applied. The load is expressed as a multiple of the initial buckling load. The displacements shown are those of the two surfaces of the shell at the impacted point. They show clearly how these surfaces, even separated by a central delamination, stay together and do not "open up" as is often assumed for flat plates. This is characteristic of cylindrical shells which always buckle "inwards" to decrease the local curvature, and the FE predictions mimicked the tests exactly. As the load is applied there is an outward displacement due to Poisson effect but at 0.6 of the buckling load there is a snap-through in stages into the post-buckled region and then a "snap-back" at a load factor of 1.3. This corresponds to a mode change as indicated in the figure, and confirms the utility of using a dynamic explicit strategy.

Simulation condition		Failure Load kN
Eigenvalue Initial buckling	No delamination	208.2
	Delaminated	158.2
Incremental compressive loading	Impact damaged, no delamination	186.9
	Delaminated	124.5
	With fibre degradation	65.4

Table 1. Failure loads for curved panel, 2mm thick.

One of the advantages of a numerical model is that the separate effects of the various failure mechanisms can be assessed as indicated in Table 1. The first eigenvalue gave the buckling of the perfect panel as 208.2kN. If the central delamination is included the increased flexibility reduces this to 158.2kN. Simulating the CAI loading of the impact damaged panel shows a failure load of 186.9Kn, but by including the delamination this is reduced to 124.5kN. Now when the panel is loaded, due to the damage producing an eccentricity, there is further local bending and fibre failure before panel failure at a load of 65.4kN. The only omission in

the simulation was propagation of the delamination front during loading, and this is currently being worked upon.The experimental failure load was 51kN. This is a fairly massive reduction from the undamaged failure load.

6. FAILURE OF COMPRESSION PANELS DUE TO STIFFENER DEBONDING

The success in modelling the previous example was somewhat fortuitous since the delamination propagation was clearly unstable under compression loading. This may not always happen, so we have looked at the pros and cons of evaluating SERR directly or by using interface elements, especially for geometrically complex configurations. The example quoted here is that of a post-buckled compression panel with "J" stiffeners. It was decided to use the global/local approach, i.e. use a fairly crude FE model to buckle the panel and then find local internal forces and moments to be applied to a 2-D plane strain section at either the nodal lines or the buckled crests of the panel. Figure 16 shows that the twisting moments for example peak at the node lines whilst the bending moments and axial forces peak at the buckled crests as shown more clearly in Figure 17 where the compressive stresses have been shed to the stiffeners as the panel buckles. These local membrane forces were then applied to the very fine mesh section shown in Figure 18 to see if failure could be predicted. This particular stiffener design had used tapered flanges to eliminate the through-thickness shear stresses at the flange edge, and which would cause failure at the node lines. Failure this time originated in the base "noodle". The SERR was found directly by using virtual crack extension at selected points. In this case we had been able to take a test panel and section it after failure showing that the stiffener debonding had started in the triangular noodle region at the base of the stiffener. We have therefore evaluated the SERR along the experimentally observed line shown in the figure and using forces/moments at the applied load which caused failure in the test. In this case no coupling between the global and the local displacements was allowed. The SERR increases dramatically as the crack opens, reaching the critical values of G_{IC} in 5mm. Thereafter the value for soft loading (load control) soars to more than 1250J/m^2 whilst the hard loading (displacement control) peaks at 700J/m^2 which is still three times the critical value. The soft loading does decrease the SERR after the peak but never becomes lower than the critical value even when the debond is complete. The other curves in the figure shown were to investigate the effect of using a high or low value of filler in the noodle insert. It turned out not to be a sensitive parameter but the shape of the noodle is much more influential, showing that a precisely machined insert is necessary.

The mesh used in this local model is probably much finer than needed, but we wished to see how high the tensile (mode I) stresses were at the flange/noodle interface. They turned out to be 40Mpa maximum in the region of the crack starter. This is lower than the expected resin strength of 50-55Mpa. This is one disadvantage of the direct method used in a true fracture mechanics strategy, i.e. how do we start the crack. We should also admit that the selection of the virtual crack zone is a non-trivial exercise, certainly it is difficult to make it an automatic procedure based solely on local stress concentrations. We therefore advocate the use of interface elements, which have the initiation routine embedded in them, but with a word of caution in conclusion

In any structure where a localised zone undergoes softening, the usual implicit algorithms may not converge, even when the "arc-length" method is used. To illustrate this we show the very simple double cantilever beam test specimen loaded to precipitate a mode 1 unstable fracture. If the chosen FE mesh is too coarse then an element sitting astride the loading/unloading ridge of Figure 1 may have two Gauss points, one on the stiffening side and the other on the softening side. It is possible for the structure to temporarily unload back towards the origin before returning to the current branch as shown in Figure 19. The only way to avoid this is to use a fine mesh so that more than two Gauss points are situated in the process

zone. This is a high price to pay for the implicit strategy which needs to satisfy equilibrium at every load increment. We would therefore advocate the robust explicit method which does not need to satisfy equilibrium at every stage. This research is ongoing.

7. CONCLUSIONS

- In-plane failure (strength criterion) and out-of-plane failure (delamination) need to be treated differently (but simultaneously if necessary.)
- Both forms may initiate and then propagate before structural failure, so any initiation stress or initiation fracture criterion will be conservative.
- Failure routines and location of sources will need to be virtually automatic to be accepted as a design tool.
- Explicit solvers and interface elements lend themselves naturally to automation.
- Virtual testing of components and substructures needs to establish credibility, or at the very least pin-point essential tests

8. ACKNOWLEDGEMENTS

We would like gratefully to acknowledge the sponsors of the various research projects summarised here. BAESystems for the work on structures with holes, and the post-buckled panels; the Ministry of Defence for the sandwich panels; and the European Commission for the curved panel work

9. REFERENCES

1. AGARD Report 772. "Analytical qualification of aircraft structures.". *70th meeting of S & M panel.* Sorrento. April 1990.

2. Soutis C, Curtis P T, and Fleck N A. "Compressive failure of notched carbon fibre composites.". *Proc. Roy. Soc. London. Series A.* **440.** 1993. Pp 241-256.

3. Gotsis P K, Chamis C C, Minnetyan. " Prediction of composite laminate fracture." *Composite Science and Technology.* **58.** No. 7.1998. Pp1137-1149

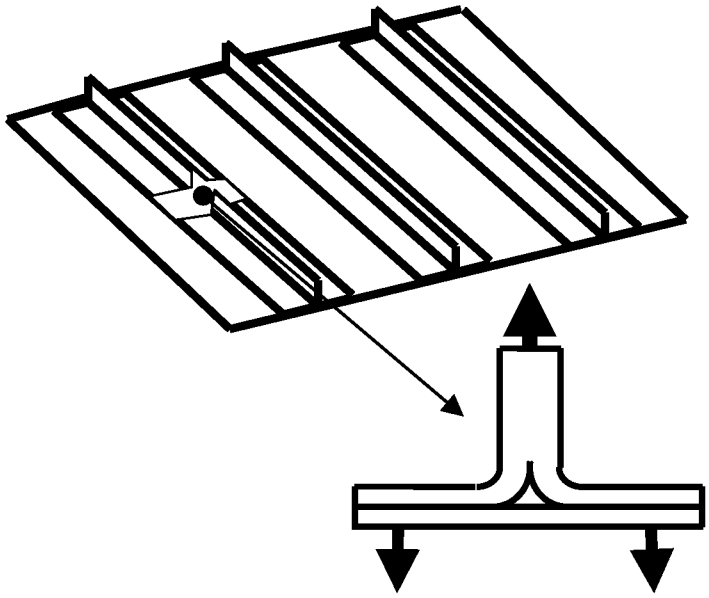

Fig.1. Global and local strategy

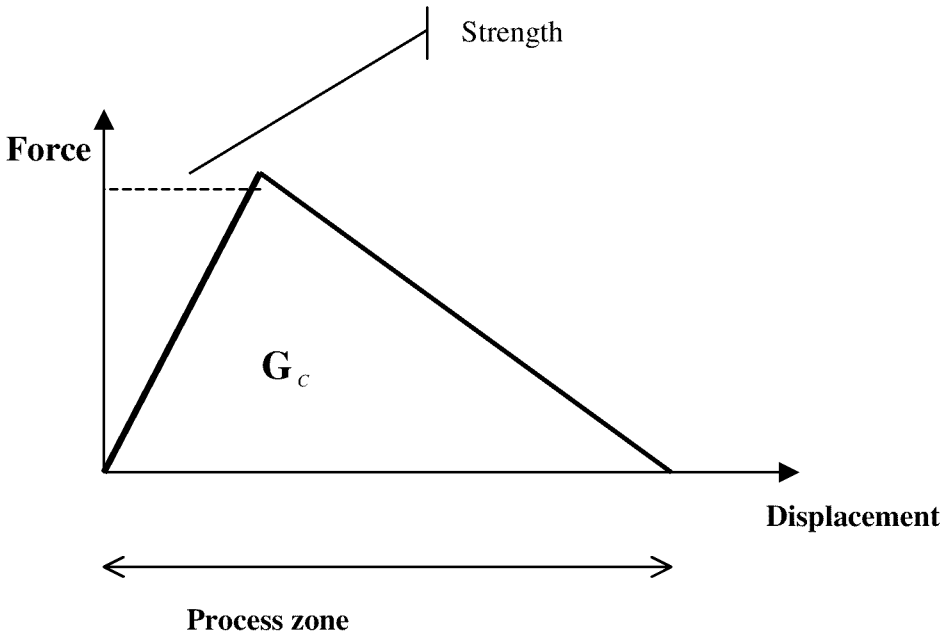

Fig. 2. Force/displacement law for interface element

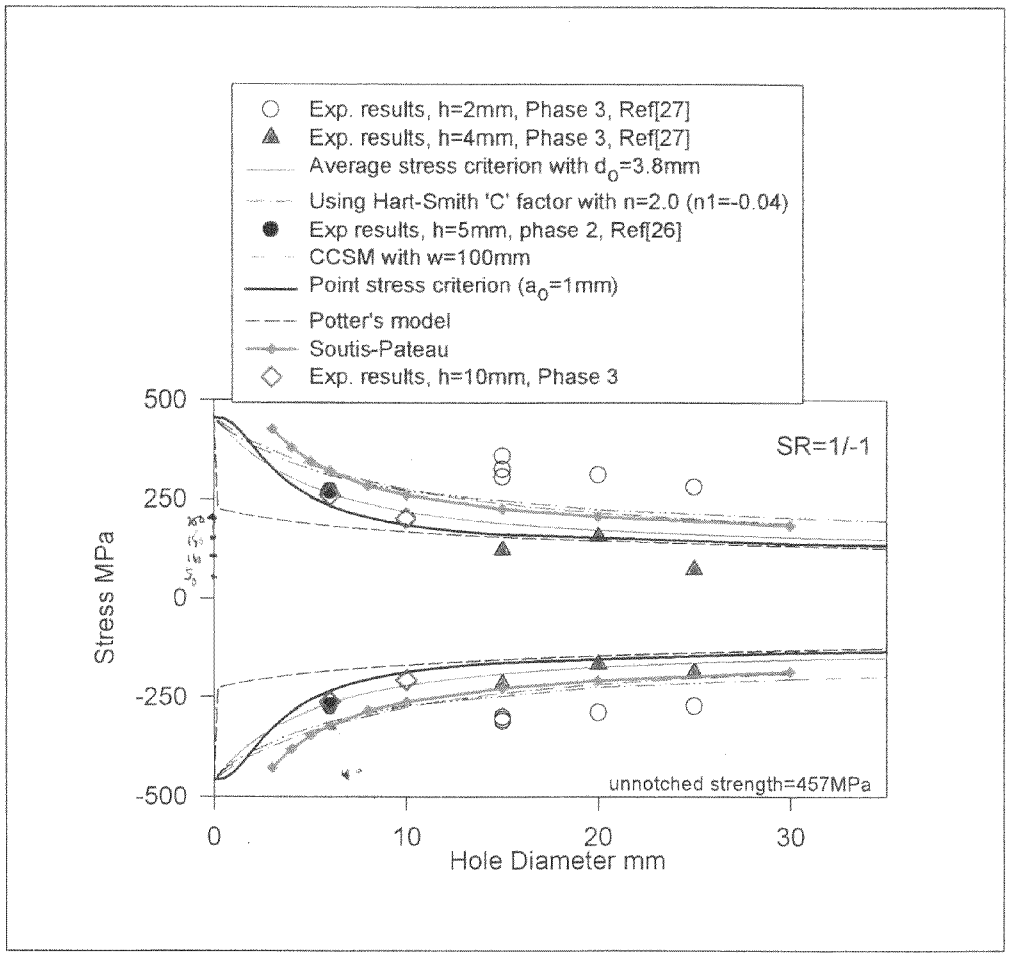

Fig. 3. Various common theoretical predictors for strength of notched composites with increasing hole size

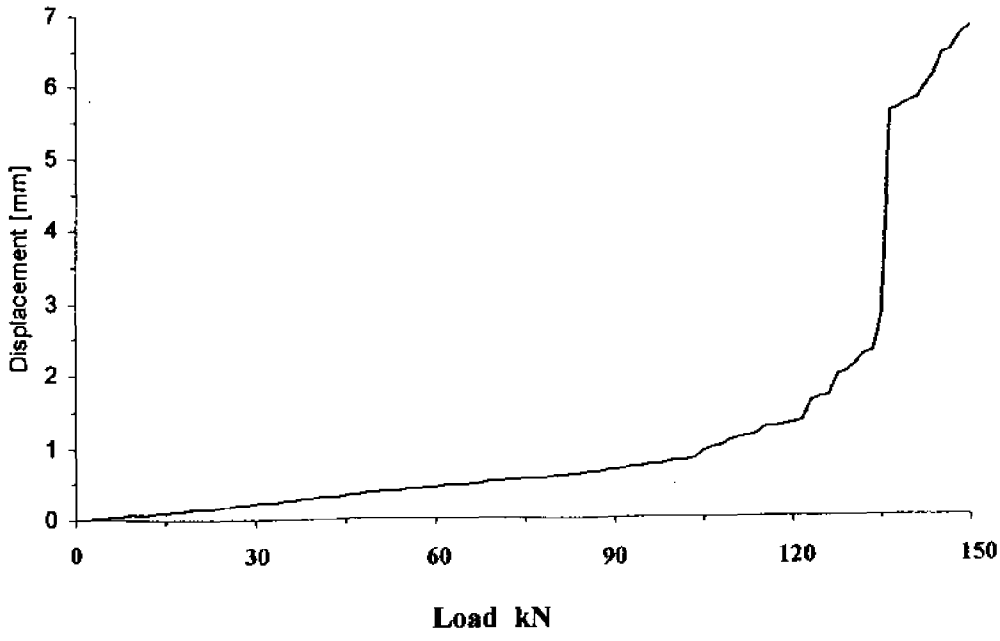

Fig. 4. Load against displacement for structure with circular hole.

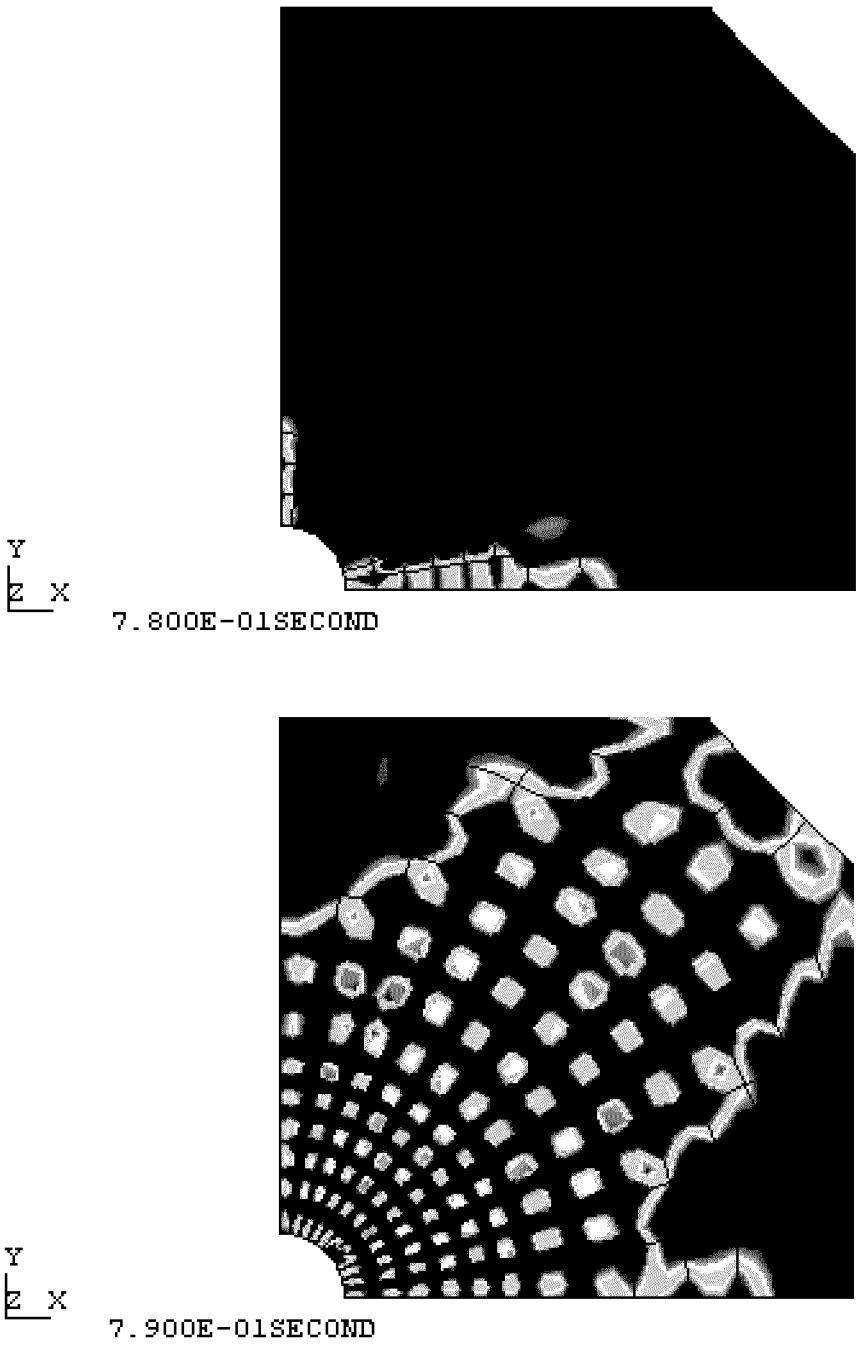

Fig. 5. A 1/4 of plate with circular hole subjected to bi-axial stress field.
In-plane damage maps at initiation and at final failure

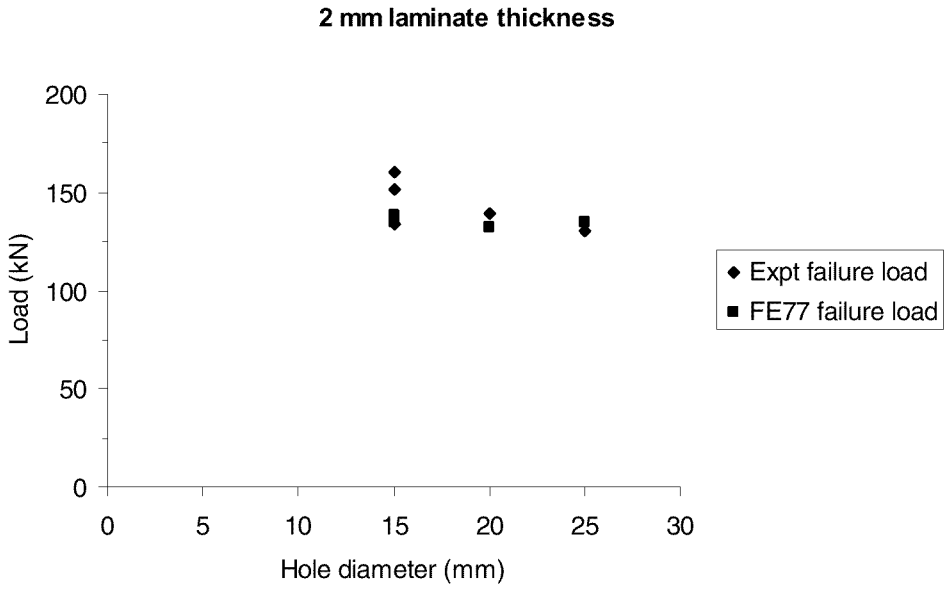

Fig. 6. Effect of notch size on strength of structure with circular holes.

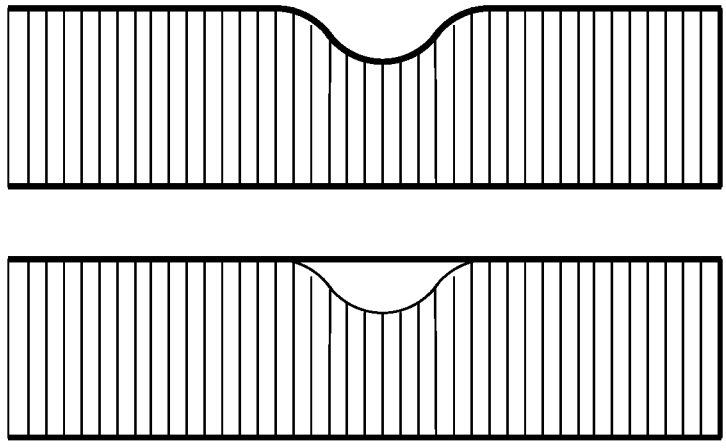

Fig. 7(a) Permanent skin indentation

Fig. 7(b) Skin recovers

Fig. 7. Possible results of impact on sandwich structure with ductile core

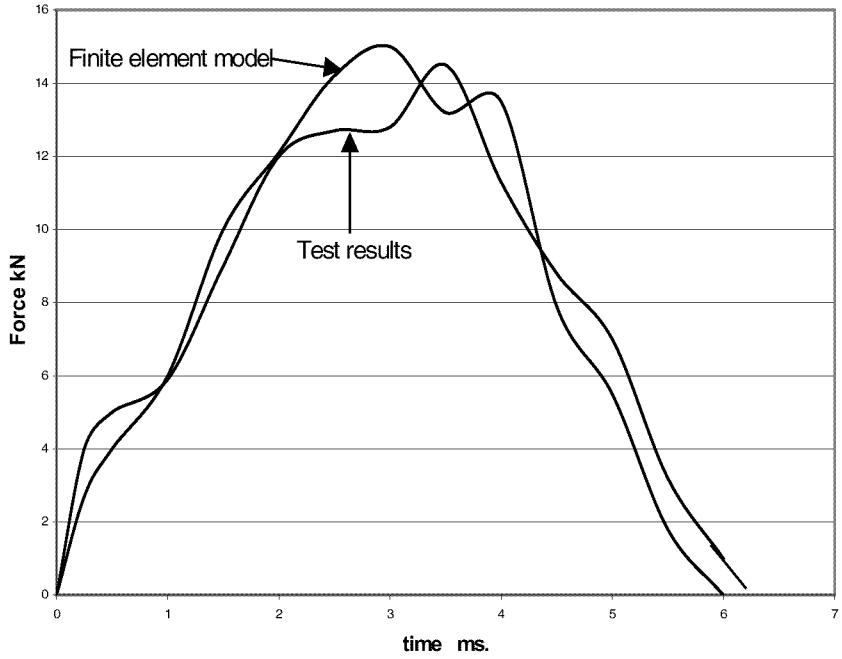

Fig. 8. Sandwich panel: impact force histories

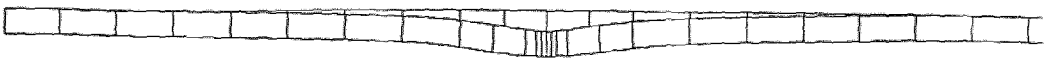

Fig. 9. Section through F.E.-predicted displacement right across panel.

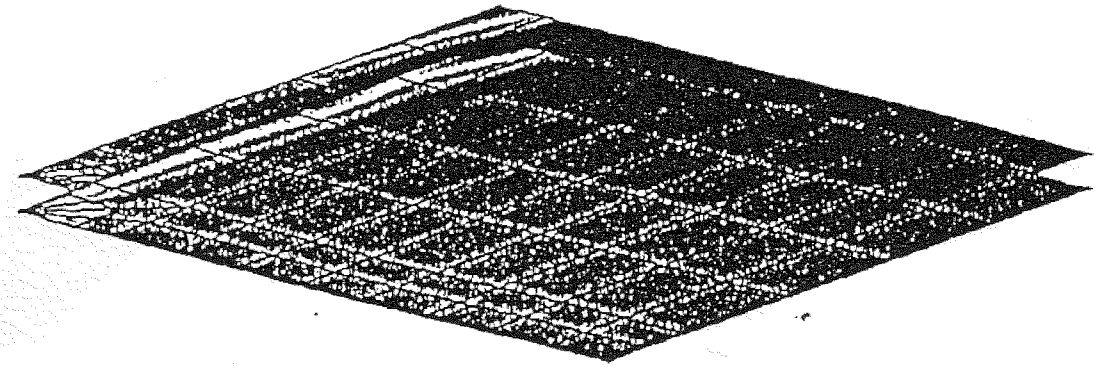

(lower skin shown is impacted front-face.)

Fig. 10. F.E.-predicted fibre damage at panel failure.

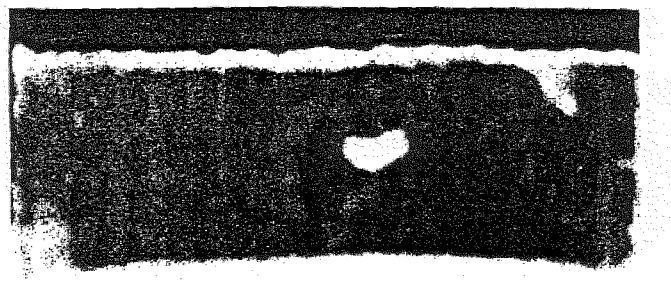

Fig. 11. C-scan revealing extent of crushed aluminium honeycomb core.

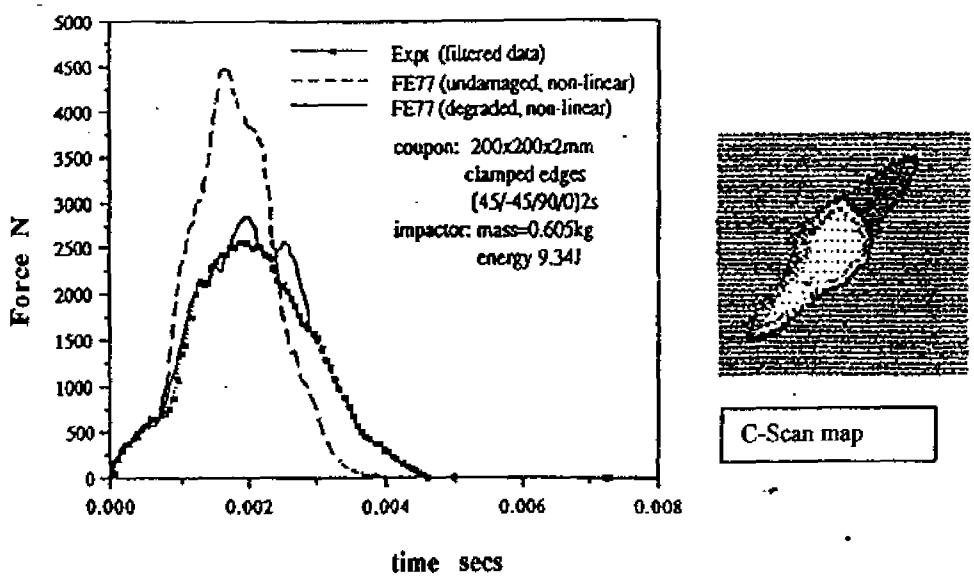

Fig. 12. Impact force history with significant fibre damage and splitting / delamination on back face.

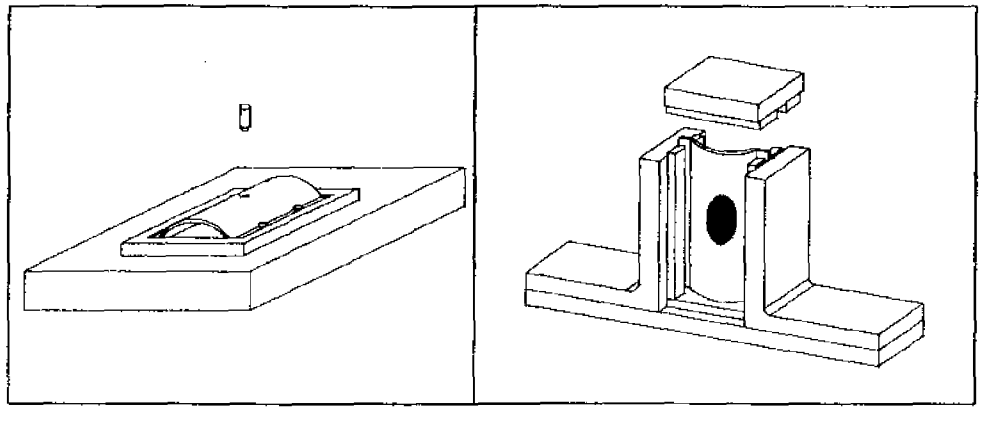

Fig. 13. Impact and C A I rigs for curved panels.

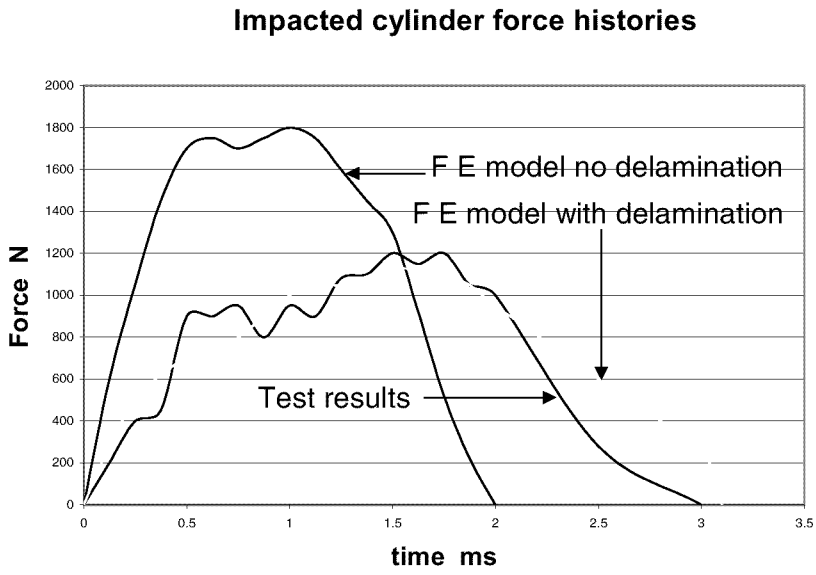

Fig. 14. Force history for curved panel with and without delamination

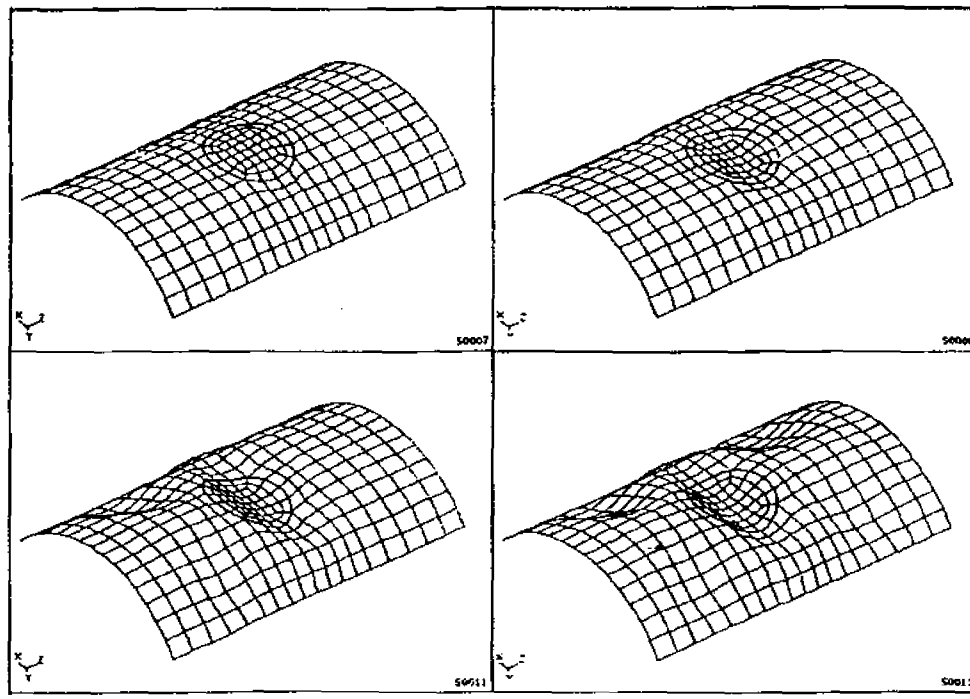

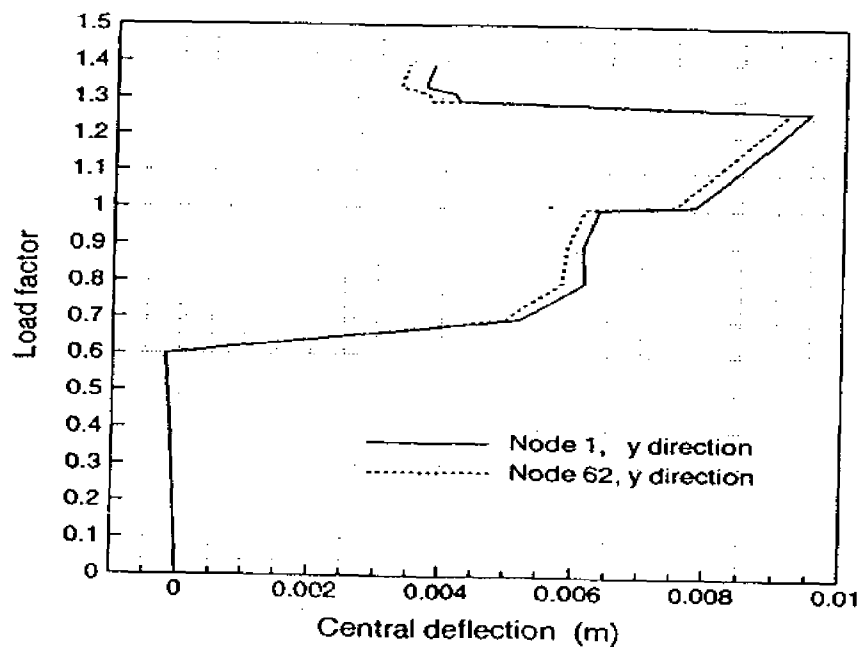

Fig. 15. F.E. model during C A I loading.

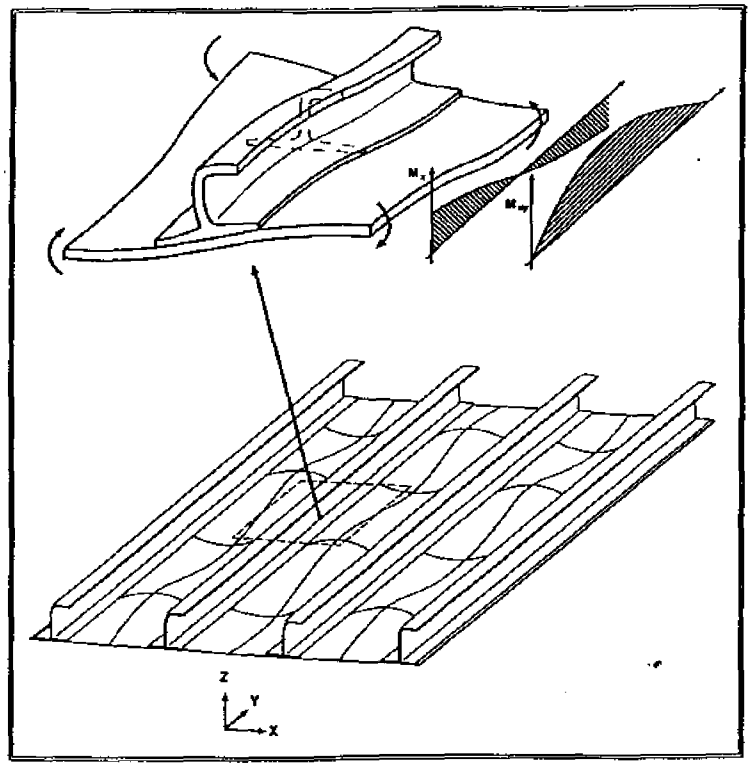

Fig. 16. Variation of bending and twisting moments along a post-buckled compression panel.

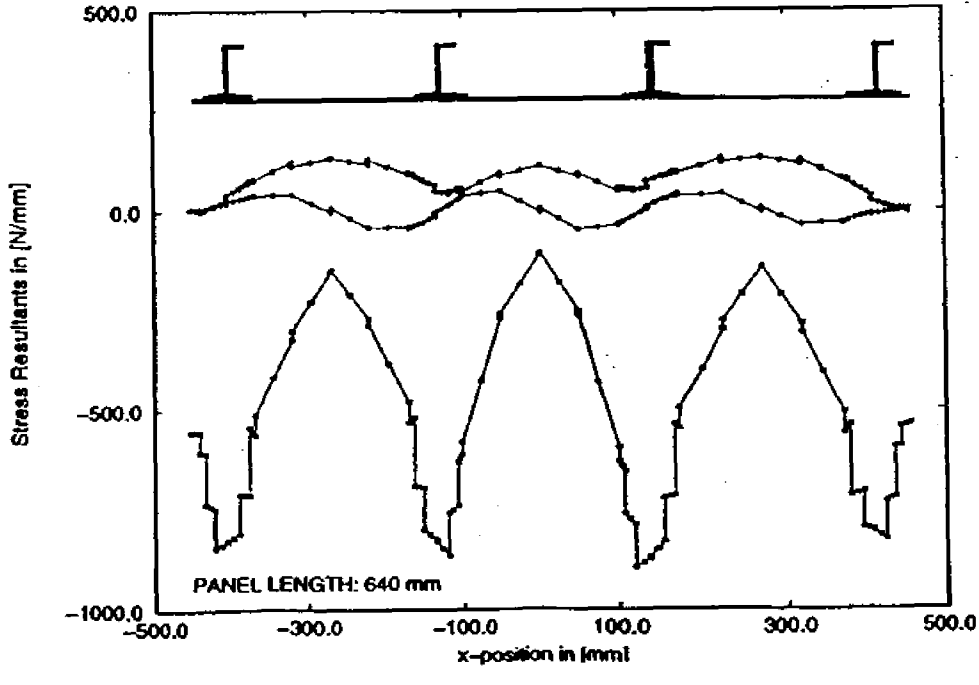

Fig. 17. Membrane compressive and shear stress resultants across buckled crest of stiffened panel.

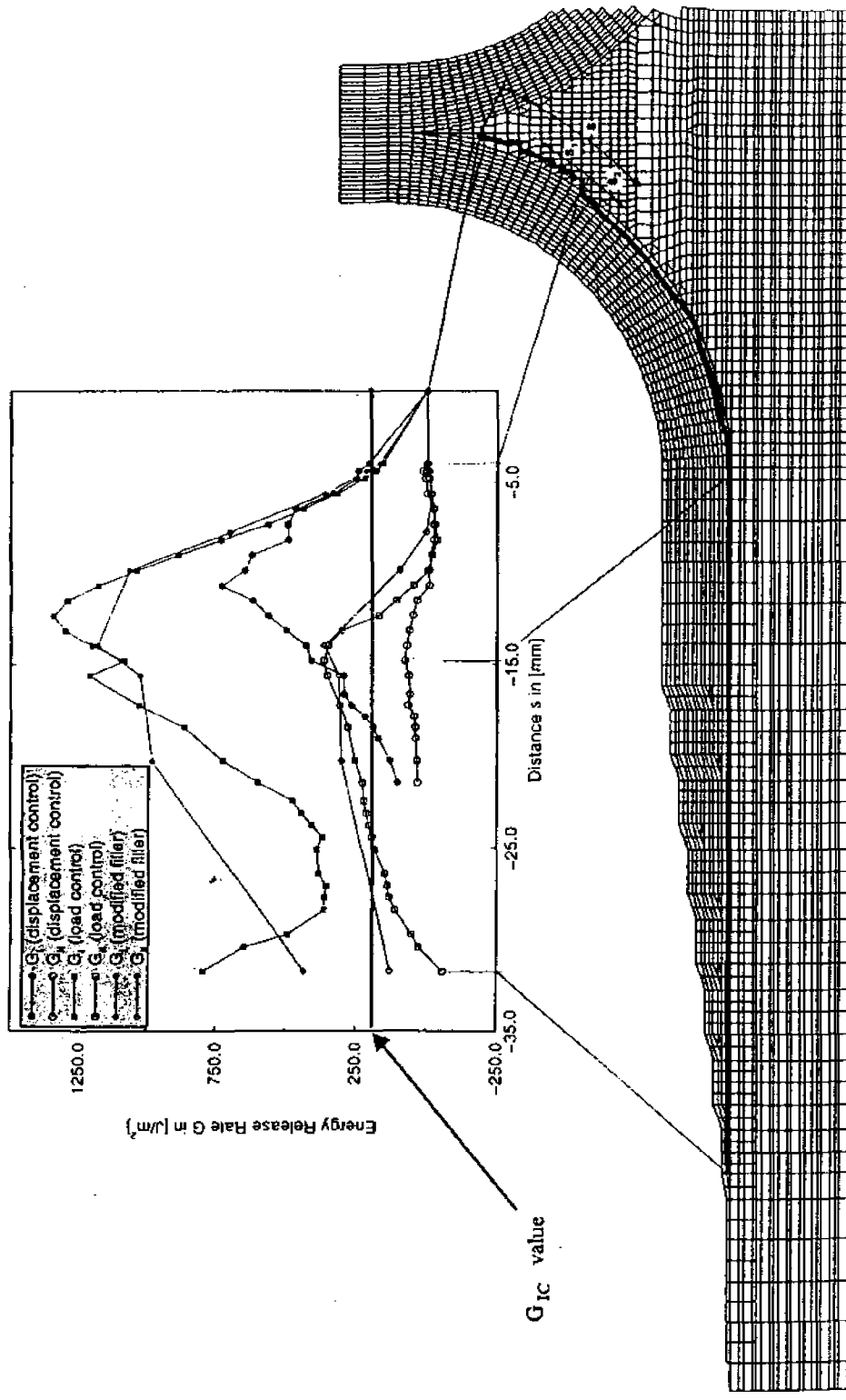

Fig. 18. F.E. model of (noodle) detail at base of stiffener.